Research Article | Vol. 8, No. 11 | 1 Nov 2017 | BIOMEDICAL OPTICS EXPRESS 4987
Biomedical Optics EXPRESS

Cerebral time domain-NIRS: reproducibility analysis, optical properties, hemoglobin species and tissue oxygen saturation in a cohort of adult subjects

GIACOMO GIACALONE,[1,2,*] MARTA ZANOLETTI,[3] DAVIDE CONTINI,[3] REBECCA RE,[3] LORENZO SPINELLI,[4] LUISA ROVERI,[1,2,5] AND ALESSANDRO TORRICELLI[3,4,5]

[1]*San Raffaele Scientific Institute, Neurology Department, Via Olgettina 60, 20132, Milan, Italy*
[2]*University "Vita-Salute" San Raffaele, Via Olgettina 60, 20132, Milan, Italy*
[3]*Politecnico di Milano, Dipartimento di Fisica, Piazza Leonardo da Vinci 32, 20133 Milan, Italy*
[4]*Istituto di Fotonica e Nanotecnologie, Consiglio Nazionale delle Ricerche, Piazza Leonardo da Vinci 32, 20133 Milan, Italy*
[5]*These authors contributed equally to this paper*
**giacalone.giacomo@hsr.it*

Abstract: The reproducibility of cerebral time-domain near-infrared spectroscopy (TD-NIRS) has not been investigated so far. Besides, reference intervals of cerebral optical properties, of absolute concentrations of deoxygenated-hemoglobin (HbR), oxygenated-hemoglobin (HbO), total hemoglobin (HbT) and tissue oxygen saturation (StO_2) and their variability have not been reported. We have addressed these issues on a sample of 88 adult healthy subjects. TD-NIRS measurements at 690, 785, 830 nm were fitted with the diffusion model for semi-infinite homogenous media. Reproducibility, performed on 3 measurements at 5 minutes intervals, ranges from 1.8 to 6.9% for each of the hemoglobin species. The mean ± SD global values of HbR, HbO, HbT, StO_2 are respectively 24 ± 7 μM, 33.3 ± 9.5 μM, 57.4 ± 15.8 μM, 58 ± 4.2%. StO_2 displays the narrowest range of variability across brain regions.

OCIS codes: (170.5280) Photon migration; (170.3660) Light propagation in tissues; (170.6935) Tissue characterization; (300.6500) Spectroscopy, time-resolved; (120.3890) Medical optics instrumentation; (170.1470) Blood or tissue constituent monitoring

References and links

1. F. F. Jöbsis, "Noninvasive, infrared monitoring of cerebral and myocardial oxygen sufficiency and circulatory parameters," Science **198**(4323), 1264–1267 (1977).
2. H. Obrig, "NIRS in clinical neurology - a 'promising' tool?" Neuroimage **85**(Pt 1), 535–546 (2014).
3. A. I. Maas and G. Citerio, "Noninvasive monitoring of cerebral oxygenation in traumatic brain injury: a mix of doubts and hope," Intensive Care Med. **36**(8), 1283–1285 (2010).
4. D. Canova, S. Roatta, D. Bosone, and G. Micieli, "Inconsistent detection of changes in cerebral blood volume by near infrared spectroscopy in standard clinical tests," J. Appl. Physiol. **110**(6), 1646–1655 (2011).
5. I. Tachtsidis and F. Scholkmann, "False positives and false negatives in functional near-infrared spectroscopy : issues, challenges, and the way forward," Neurophotonics **3**(3), 031405 (2016).
6. F. Scholkmann, S. Kleiser, A. J. Metz, R. Zimmermann, J. Mata Pavia, U. Wolf, and M. Wolf, "A review on continuous wave functional near-infrared spectroscopy and imaging instrumentation and methodology," NeuroImage **85**, 6–27 (2014).
7. A. Torricelli, D. Contini, A. Pifferi, M. Caffini, R. Re, L. Zucchelli, and L. Spinelli, "Time domain functional NIRS imaging for human brain mapping," Neuroimage **85**(Pt 1), 28–50 (2014).
8. H. Auger, L. Bherer, É. Boucher, R. Hoge, F. Lesage, and M. Dehaes, "Quantification of extra-cerebral and cerebral hemoglobin concentrations during physical exercise using time-domain near infrared spectroscopy," Biomed. Opt. Express **7**(10), 3826–3842 (2016).
9. L. Gagnon, C. Gauthier, R. D. Hoge, F. Lesage, J. Selb, and D. A. Boas, "Double-layer estimation of intra- and extracerebral hemoglobin concentration with a time-resolved system," J. Biomed. Opt. **13**(5), 054019 (2008).
10. V. Quaresima, M. Ferrari, A. Torricelli, L. Spinelli, A. Pifferi, and R. Cubeddu, "Bilateral prefrontal cortex

#303593 https://doi.org/10.1364/BOE.8.004987
Journal © 2017 Received 28 Jul 2017; revised 14 Sep 2017; accepted 22 Sep 2017; published 12 Oct 2017

Biomedical Optics EXPRESS

oxygenation responses to a verbal fluency task: a multichannel time-resolved near-infrared topography study," J. Biomed. Opt. **10**(1), 011012 (2005).
11. B. Hallacoglu, A. Sassaroli, M. Wysocki, E. Guerrero-Berroa, M. Schnaider Beeri, V. Haroutunian, M. Shaul, I. H. Rosenberg, A. M. Troen, and S. Fantini, "Absolute measurement of cerebral optical coefficients, hemoglobin concentration and oxygen saturation in old and young adults with near-infrared spectroscopy," J. Biomed. Opt. **17**(8), 081406 (2012).
12. R. Gatto, W. E. Hoffman, M. Mueller, C. Paisansathan, and F. Charbel, "Age effects on brain oxygenation during hypercapnia," J. Biomed. Opt. **12**(6), 062113 (2007).
13. J. Choi, M. Wolf, V. Toronov, U. Wolf, C. Polzonetti, D. Hueber, L. P. Safonova, R. Gupta, A. Michalos, W. Mantulin, and E. Gratton, "Noninvasive determination of the optical properties of adult brain: near-infrared spectroscopy approach," J. Biomed. Opt. **9**(1), 221–229 (2004).
14. F. Moreau, R. Yang, V. Nambiar, A. M. Demchuk, and J. F. Dunn, "Near-infrared measurements of brain oxygenation in stroke," Neurophotonics **3**(3), 031403 (2016).
15. D. Comelli, A. Bassi, A. Pifferi, P. Taroni, A. Torricelli, R. Cubeddu, F. Martelli, and G. Zaccanti, "In vivo time-resolved reflectance spectroscopy of the human forehead," Appl. Opt. **46**(10), 1717–1725 (2007).
16. A. Farina, A. Torricelli, I. Bargigia, L. Spinelli, R. Cubeddu, F. Foschum, M. Jäger, E. Simon, O. Fugger, A. Kienle, F. Martelli, P. Di Ninni, G. Zaccanti, D. Milej, P. Sawosz, M. Kacprzak, A. Liebert, and A. Pifferi, "In-vivo Multilaboratory investigation of the optical properties of the human head," Biomed. Opt. Express **6**(7), 2609–2623 (2015).
17. J. W. Bartlett and C. Frost, "Reliability, repeatability and reproducibility: analysis of measurement errors in continuous variables," Ultrasound Obstet. Gynecol. **31**(4), 466–475 (2008).
18. B. N. Taylor and C. E. Kuyatt, "National Institute for Standards and Technology Technical Note 1297 - Guidelines for Evaluating and Expressing the Uncertainty of NIST Measurement Results," https://www.nist.gov/pml/nist-technical-note-1297
19. C. Jenny, M. Biallas, I. Trajkovic, J. C. Fauchère, H. U. Bucher, and M. Wolf, "Reproducibility of cerebral tissue oxygen saturation measurements by near-infrared spectroscopy in newborn infants," J. Biomed. Opt. **16**(9), 097004 (2011).
20. S. J. Arri, T. Muehlemann, M. Biallas, H. U. Bucher, and M. Wolf, "Precision of cerebral oxygenation and hemoglobin concentration measurements in neonates measured by near-infrared spectroscopy," J. Biomed. Opt. **16**(4), 047005 (2011).
21. L. C. Sorensen and G. Greisen, "Precision of measurement of cerebral tissue oxygenation index using near-infrared spectroscopy in preterm neonates," J. Biomed. Opt. **11**(5), 054005 (2006).
22. A. Dullenkopf, A. Kolarova, G. Schulz, B. Frey, O. Baenziger, and M. Weiss, "Reproducibility of cerebral oxygenation measurement in neonates and infants in the clinical setting using the NIRO 300 oximeter," Pediatr. Crit. Care Med. **6**(3), 344–347 (2005).
23. T. W. Hessel, S. Hyttel-Sorensen, and G. Greisen, "Cerebral oxygenation after birth - a comparison of INVOS and FORE-SIGH near-infrared spectroscopy oximeters," Acta Paediatr. **103**(5), 488–493 (2014).
24. J. Menke, U. Voss, G. Möller, and G. Jorch, "Reproducibility of cerebral near infrared spectroscopy in neonates," Biol. Neonate **83**(1), 6–11 (2003).
25. Royal College of Physicians, "Research on healthy subjects," J R Coll Physicians **20**, 243–257 (1986).
26. International Elettrotechnical Commision, *Safety of laser products - Part 1: Equipment classification and requirements*, Edition 2 (2007).
27. A. Pifferi, A. Torricelli, A. Bassi, P. Taroni, R. Cubeddu, H. Wabnitz, D. Grosenick, M. Möller, R. Macdonald, J. Swartling, T. Svensson, S. Andersson-Engels, R. L. van Veen, H. J. Sterenborg, J. M. Tualle, H. L. Nghiem, S. Avrillier, M. Whelan, and H. Stamm, "Performance assessment of photon migration instruments: the MEDPHOT protocol," Appl. Opt. **44**(11), 2104–2114 (2005).
28. H. Wabnitz, A. Jelzow, M. Mazurenka, O. Steinkellner, R. Macdonald, D. Milej, N. Żołek, M. Kacprzak, P. Sawosz, R. Maniewski, A. Liebert, S. Magazov, J. Hebden, F. Martelli, P. Di Ninni, G. Zaccanti, A. Torricelli, D. Contini, R. Re, L. Zucchelli, L. Spinelli, R. Cubeddu, and A. Pifferi, "Performance assessment of time-domain optical brain imagers, part 2: nEUROPt protocol," J. Biomed. Opt. **19**(8), 086012 (2014).
29. L. Koessler, L. Maillard, A. Benhadid, J. P. Vignal, J. Felblinger, H. Vespignani, and M. Braun, "Automated cortical projection of EEG sensors: anatomical correlation via the international 10-10 system," Neuroimage **46**(1), 64–72 (2009).
30. L. Tatu, T. Moulin, J. Bogousslavsky, and H. Duvernoy, "Arterial territories of the human brain: cerebral hemispheres," Neurology **50**(6), 1699–1708 (1998).
31. D. Contini, F. Martelli, and G. Zaccanti, "Photon migration through a turbid slab described by a model based on diffusion approximation. I. Theory," Appl. Opt. **36**(19), 4587–4599 (1997).
32. C. D'Andrea, L. Spinelli, A. Bassi, A. Giusto, D. Contini, J. Swartling, A. Torricelli, and R. Cubeddu, "Time-resolved spectrally constrained method for the quantification of chromophore concentrations and scattering parameters in diffusing media," Opt. Express **14**(5), 1888–1898 (2006).
33. A. M. Nilsson, C. Sturesson, D. L. Liu, and S. Andersson-Engels, "Changes in spectral shape of tissue optical properties in conjunction with laser-induced thermotherapy," Appl. Opt. **37**(7), 1256–1267 (1998).
34. J. R. Mourant, T. Fuselier, J. Boyer, T. M. Johnson, and I. J. Bigio, "Predictions and measurements of scattering and absorption over broad wavelength ranges in tissue phantoms," Appl. Opt. **36**(4), 949–957 (1997).
35. J. M. Bland and D. G. Altman, "Measurement error," BMJ **312**(7047), 1654 (1996).

Biomedical Optics EXPRESS

36. S. Vaz, T. Falkmer, A. E. Passmore, R. Parsons, and P. Andreou, "The case for using the repeatability coefficient when calculating test-retest reliability," PLoS One **8**(9), e73990 (2013).
37. T. Alderliesten, L. Dix, W. Baerts, A. Caicedo, S. van Huffel, G. Naulaers, F. Groenendaal, F. van Bel, and P. Lemmers, "Reference values of regional cerebral oxygen saturation during the first 3 days of life in preterm neonates," Pediatr. Res. **79**(1-1), 55–64 (2016).
38. A. Chieregato, F. Calzolari, G. Trasforini, L. Targa, and N. Latronico, "Normal jugular bulb oxygen saturation," J. Neurol. Neurosurg. Psychiatry **74**(6), 784–786 (2003).
39. E. L. Gibbs, W. G. Lennox, and L. F. Nims, "Arterial and cerebral venous blood. Arterial-venous differences in man," J. Biol. Chem. **144**, 325–332 (1942).
40. H. Ito, I. Kanno, H. Iida, J. Hatazawa, E. Shimosegawa, H. Tamura, and T. Okudera, "Arterial fraction of cerebral blood volume in humans measured by positron emission tomography," Ann. Nucl. Med. **15**(2), 111–116 (2001).
41. P. Pantano, J. C. Baron, P. Lebrun-Grandié, N. Duquesnoy, M. G. Bousser, and D. Comar, "Regional cerebral blood flow and oxygen consumption in human aging," Stroke **15**(4), 635–641 (1984).
42. J. Zhang, T. Liu, A. Gupta, P. Spincemaille, T. D. Nguyen, and Y. Wang, "Quantitative mapping of cerebral metabolic rate of oxygen ($CMRO_2$) using quantitative susceptibility mapping (QSM)," Magn. Reson. Med. **74**(4), 945–952 (2015).
43. M. E. Raichle, A. M. MacLeod, A. Z. Snyder, W. J. Powers, D. A. Gusnard, and G. L. Shulman, "A default mode of brain function," Proc. Natl. Acad. Sci. U.S.A. **98**(2), 676–682 (2001).
44. B. Biswal, F. Z. Yetkin, V. M. Haughton, and J. S. Hyde, "Functional connectivity in the motor cortex of resting human brain using echo-planar MRI," Magn. Reson. Med. **34**(4), 537–541 (1995).
45. S. Sasai, F. Homae, H. Watanabe, A. T. Sasaki, H. C. Tanabe, N. Sadato, and G. Taga, "A NIRS-fMRI study of resting state network," Neuroimage **63**(1), 179–193 (2012).
46. H. Yuan, V. Zotev, R. Phillips, W. C. Drevets, and J. Bodurka, "Spatiotemporal dynamics of the brain at rest-Exploring EEG microstates as electrophysiological signatures of BOLD resting state networks," Neuroimage **60**(4), 2062–2072 (2012).
47. S. G. Horovitz, M. Fukunaga, J. A. de Zwart, P. van Gelderen, S. C. Fulton, T. J. Balkin, and J. H. Duyn, "Low frequency BOLD fluctuations during resting wakefulness and light sleep: a simultaneous EEG-fMRI study," Hum. Brain Mapp. **29**(6), 671–682 (2008).
48. M. Ibaraki, Y. Shinohara, K. Nakamura, S. Miura, F. Kinoshita, and T. Kinoshita, "Interindividual variations of cerebral blood flow, oxygen delivery, and metabolism in relation to hemoglobin concentration measured by positron emission tomography in humans," J. Cereb. Blood Flow Metab. **30**(7), 1296–1305 (2010).
49. Y. Zhao, J. Wen, A. H. Cross, and D. A. Yablonskiy, "On the relationship between cellular and hemodynamic properties of the human brain cortex throughout adult lifespan," Neuroimage **133**, 417–429 (2016).
50. T. Yamaguchi, I. Kanno, K. Uemura, F. Shishido, A. Inugami, T. Ogawa, M. Murakami, and K. Suzuki, "Reduction in regional cerebral metabolic rate of oxygen during human aging," Stroke **17**(6), 1220–1228 (1986).
51. K. L. Leenders, D. Perani, A. A. Lammertsma, J. D. Heather, P. Buckingham, M. J. Healy, J. M. Gibbs, R. J. Wise, J. Hatazawa, S. Herold, R. P. Beaney, D. J. Brooks, T. Spinks, C. Rhodes, and R. S. J. Frackowiak, "Cerebral blood flow, blood volume and oxygen utilization. Normal values and effect of age," Brain **113**(1), 27–47 (1990).
52. F. Wenz, K. Rempp, G. Brix, M. V. Knopp, F. Gückel, T. Hess, and G. van Kaick, "Age dependency of the regional cerebral blood volume (rCBV) measured with dynamic susceptibility contrast MR imaging (DSC)," Magn. Reson. Imaging **14**(2), 157–162 (1996).
53. G. Marchal, P. Rioux, M. C. Petit-Taboué, G. Sette, J. M. Travère, C. Le Poec, P. Courtheoux, J. M. Derlon, and J. C. Baron, "Regional cerebral oxygen consumption, blood flow, and blood volume in healthy human aging," Arch. Neurol. **49**(10), 1013–1020 (1992).
54. J. J. Chen, H. D. Rosas, and D. H. Salat, "Age-associated reductions in cerebral blood flow are independent from regional atrophy," Neuroimage **55**(2), 468–478 (2011).
55. C. C. Meltzer, M. N. Cantwell, P. J. Greer, D. Ben-Eliezer, G. Smith, G. Frank, W. H. Kaye, P. R. Houck, and J. C. Price, "Does cerebral blood flow decline in healthy aging? A PET study with partial-volume correction," J. Nucl. Med. **41**(11), 1842–1848 (2000).
56. C. Wu, A. R. Honarmand, S. Schnell, R. Kuhn, S. E. Schoeneman, S. A. Ansari, J. Carr, M. Markl, and A. Shaibani, "Age-related changes of normal cerebral and cardiac blood flow in children and adults aged 7 months to 61 years," J. Am. Heart Assoc. **5**(1), 1–14 (2016).
57. J. B. De Vis, J. Hendrikse, A. Bhogal, A. Adams, L. J. Kappelle, and E. T. Petersen, "Age-related changes in brain hemodynamics; a calibrated MRI study," Hum. Brain Mapp. **36**(10), 3973–3987 (2015).
58. C. D. Good, I. S. Johnsrude, J. Ashburner, R. N. Henson, K. J. Friston, and R. S. Frackowiak, "A voxel-based morphometric study of ageing in 465 normal adult human brains," Neuroimage **14**(1), 21–36 (2001).
59. A. K. Bourisly, A. El-Beltagi, J. Cherian, G. Gejo, A. Al-Jazzaf, and M. Ismail, "A voxel-based morphometric magnetic resonance imaging study of the brain detects age-related gray matter volume changes in healthy subjects of 21-45 years old," Neuroradiol. J. **28**(5), 450–459 (2015).
60. R. I. Scahill, C. Frost, R. Jenkins, J. L. Whitwell, M. N. Rossor, and N. C. Fox, "A longitudinal study of brain volume changes in normal aging using serial registered magnetic resonance imaging," Arch. Neurol. **60**(7), 989–994 (2003).

Biomedical Optics EXPRESS

61. U. Mahlknecht and S. Kaiser, "Age-related changes in peripheral blood counts in humans," Exp. Ther. Med. **1**(6), 1019–1025 (2010).

1. Introduction

Near-infrared spectroscopy (NIRS) is a non-invasive methodology able to provide continuous monitoring of cerebral oxygenation parameters at the bed-side of the patient. Despite over 35 years have passed since its first description [1,2], NIRS application has been hindered in the routine clinical settings by a number of limiting factors (e.g. lack of absolute data, confounding effects due to systemic superficial changes or movement artifacts) [3–5]. Some limitations have been overcome thanks to the technological advances. In particular, differently from the classical continuous-wave technology (CW-NIRS) [6], the frequency- (FD-) and time-domain (TD-) NIRS [7] allow to calculate the absolute absorption and reduced scattering coefficients, to recover the absolute concentrations of hemoglobin species and to better separate the contribution of the extra-cerebral layers from the brain cortical ones.

The first steps to apply efficiently NIRS in neurology clinic should be to evaluate the *in vivo* reproducibility of the technique, to define normal values of cerebral deoxy-hemoglobin (HbR), oxy-hemoglobin (HbO), total hemoglobin (HbT) and tissue oxygen saturation (StO_2) and to assess the variability among brain areas and between hemispheres. Previous studies analyzed optical properties of adult head *in vivo* with FD- or TD-NIRS techniques on a limited number of subjects [8–16] registered exclusively from the forehead except from one study [14]. The reported ranges of normal values for HbR, HbO, HbT concentrations and StO_2 were heterogeneous (Table 1).

Reproducibility, which is defined as the variation in measurements under changing conditions such as time [17,18], has been tested *in vivo* in few studies, carried out mainly with the CW-NIRS technique (for StO_2) in neonates, with contrasting results [19–24]. The reproducibility of FD-NIRS in adult subjects was investigated in one recent study that reported correlation coefficients between measurements taken 5 months apart ranging from 0.7 to 0.9 for the hemoglobin species [11].

The aim of the present study is to assess reproducibility of TD-NIRS measurements under changing conditions of time and after removing and repositioning of the optical fibers (short-term reproducibility). In addition, we describe the variability between hemispheres and head regions and the range of normal values of TD-NIRS measurements obtained from three different head regions (frontal, central, and parietal) in a relatively large cohort of adult healthy subjects.

Table 1. Cerebral hemoglobin species: mean concentrations on adults from previous studies.

Reference	NIRS type	Position	Model	N.	Age (y)	HbR (μM)	HbO (μM)	HbT (μM)	StO_2 (%)
Auger *et al.* [8]	TD[a]	Frontal	Two-layer	30	18-30	27	38	65	58
Gagnon *et al.* [9]	TD[a]	Frontal	Two-layer	5	NR[c]	20±4	31±8	51±11	60±4
Quaresima *et al.* [10]	TD[a]	Frontal	Homogeneous	8	35+/-9	21±4	49±8	70±10	70±3
Choi *et al.* [13]	FD[b]	Frontal	Two-layer	30	20-50	20±6	56±12	76±14	74±6
Hallacoglu *et al.* [11]	FD[b]	Frontal	Homogeneous	19 36	28+/-4 85+/-6	22±2 18±1	30±3 20±1	52±13 38±2	58±9 52±2
Moreau *et al.* [14]	FD[b]	Frontal, Rolandic, Broca	Homogeneous	11	43 (35-49)	20±4	36±9	56±12	63±5
Gatto *et al* .[12]	FD[b]	Frontal	Homogeneous	13	26-59	18±7	24±8	42±14	57±7

[a]TD: Time-Domain; [b]FD: Frequency-Domain; [c]NR: not reported.

Biomedical Optics EXPRESS

2. Methods

2.1 Subjects

The study received approval of the Ethical Committee of San Raffaele Scientific Institute and the Italian Ministry of Health and was conducted in compliance with the Declaration of Helsinki. Each subject gave written informed consent. Adult healthy subjects [25] were enrolled according to the following inclusion criteria: age ≥18 years old; absence of stenosis ≥ 50% in cervical extra-cranial and intra-cranial arteries according to Doppler ultrasonography; absence on head CT- or MRI-scan, when available, of high-grade cerebral small vessel vasculopathy (Fazekas scale > 2) or other relevant pathologies.

2.2 Instrumentation and data acquisition

The TD-NIRS system was designed and developed at Politecnico di Milano. It employs pulsed diode lasers (LDH-series, PicoQuant GmbH, Germany) as light sources, operating at 690, 785 and 830 nm, with a repetition rate of 80 MHz, pulse duration of about 100 ps, and average power of <1 mW. Light pulses from the three laser diodes are coupled into three multimode graded index fibers (100/140 μm core/cladding diameter) terminated by a single SMA (SMA905) connector. A proper spacer ensures that the power density on the skin is below the maximum permissible emission limit (<2 mW/mm^2) [26]. Motor driven circular variable neutral density filters (43-770, Edmud Optics GmbH, Germany) are used to equalize the injected power. An in-house made three furcated fiber bundle, made of graded index plastic optical fibers (1 mm core diameter, 0.29 NA; OM-GIGA, Luceat Srl, Italy), is used for photon collection. Each collection fiber is coupled to an hybrid photomultipliers (HPM-100-50, Becker-Hickl GmbH, Germany) with band pass filters centered at 690, 785 and 830 nm (Hard Coated OD 4, 10 nm Bandpass Filters, Edmund Optics GmbH, Germany) for photo detection. Three Time Correlated Single Photon Counting (TCSPC) boards (SPC150, Becker&Hickl, Germany) are used for parallel acquisition of the reflectance curves. The entire system is hosted in a 19-inch rack and can be operated as medical device for research purposes. The performances of the device were fully characterized following already established protocols for photon migration instruments (e.g. BIP and MEDPHOT protocols) [27, 28]. The instrument response function (IRF), obtained facing the injection and collection fibers with a thin Teflon film in between to properly excite all modes in the fiber bundle, has a full width at half maximum (FWHM) of <200 ps. Figure 1 shows an example of IRF and of TD-NIRS data on a subject.

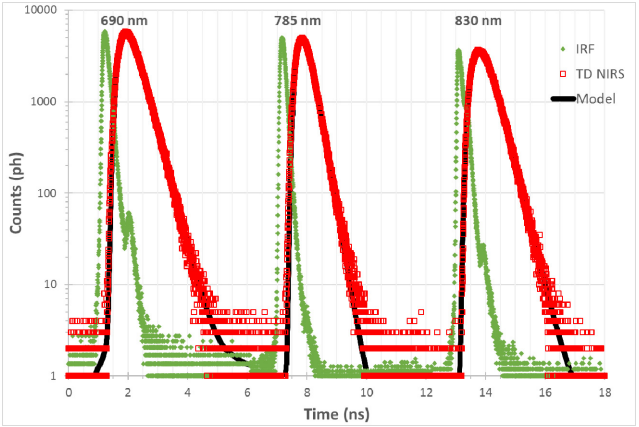

Fig. 1. IRF (green diamond) and TD-NIRS curves (red square) at 690, 785, and 830 nm respectively fitted data with a homogeneous model is also shown (black line).

Biomedical Optics EXPRESS

2.3 Measurement protocol

TD-NIRS measurements were obtained from frontal, central and parietal brain regions on each hemisphere. The optical probes were positioned by means of a modified EEG cap (g.EEGcap, g.tec medical engineering GmbH, Austria) according to the 10-10 international system (position F3-F5, C3-C1, P3-P5 for the left hemisphere and C4-C2, F4-F6, P4-P6 for the right hemisphere) and held manually to improve stability (Fig. 2). According to probabilistic anatomical correlation of 10-10 international system to the brain cortex (Koessler, 2009 [29]), these positions should investigate the following brain areas: dorsolateral prefrontal cortex [Broadman areas (BA) 9, 46] and frontal eye fields (BA 8) (frontal positions), pre- and post-central giri (primary somatosensory and motor cortices, BA 1-4) (central positions), secondary associative visual, somatosensory and auditory cortices (BA 7, 19, 39) (parietal positions). We chose these positions for two main reasons: a) to gather standardized information about equidistant areas in the territory supplied by middle cerebral artery [30]; b) to probe both primary and secondary cortices.

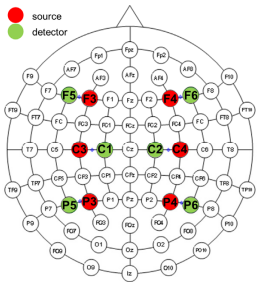

Fig. 2. Schematic representation of the international 10-10 positioning system. Bold characters indicate the 12 positions (six pairs of source and detector) selected in the study. The first letter of the position indicates the region: F stands for frontal, C for central, P for parietal region. Positions in the left hemisphere end with an odd number; an even number indicates the right hemisphere. Red and green disks represent respectively source and detector.

The injected power of each position was optimized to collect at least 10^6 photons for each wavelength in a maximum acquisition time of 30 s.

The study protocol was performed in a quiet room, in condition of low light with subject at rest laying with angle-of-bed inclination at 30°. Reproducibility of measurements was tested by performing 3 measurements at 5 minutes intervals after removing and repositioning of the optical probes (short-term reproducibility).

During the experimental session of each subject, the IRF and the TD-NIRS curves from a solid phantom [nominal optical properties at 660 nm: absorption (μ_a) 0.1 cm^{-1} and reduced scattering coefficient (μ_s') 10 cm^{-1}] were measured at least once to monitor the performances of the device. Therefore, the quality of phantom was established as the mean ± 2 standard deviations (SD) of the distribution of fitted optical properties of all measurements. Quality assessment included $\Delta t_{TDNIRS\text{-}IRF}$, the difference between the temporal position of the barycenter of TD-NIRS photon curves and the barycenter of the IRF. We then calculated the mean ± 2SD of the distribution of $\Delta t_{TDNIRS\text{-}IRF}$ for every pairs of TD-NIRS and IRF curve of the entire cohort of subjects. Then we discarded TD-NIRS curves having a $\Delta t_{TDNIRS\text{-}IRF}$ larger than 2 SD of the mean time shift (see paragraph 2.4).

2.4 Data analysis

TD-NIRS data at each wavelength were fitted with the solution of the diffusion equation for semi-infinite homogenous media after convolution with the IRF [31]. A spectral constraint during the inversion procedure was employed [32]. In particular, we used the empirical spectral dependence for the reduced scattering (obtained by Mie theory [33,34]):

Biomedical Optics EXPRESS

$$\mu_s'(\lambda) = a(\lambda / \lambda_0)^{-b} \quad (1)$$

where λ is the wavelength, λ_0 is a reference wavelength (600 nm in this case), a is the estimated reduced scattering coefficient at λ_0, b is the so called scattering power. Note that a and b can be related to the equivalent density and size of scatters [33,34]. Further, we used the Beer's law to express the absorption coefficient as a linear superposition of the specific absorption of HbR, HbO and water:

$$\mu_a(\lambda) = \varepsilon_{HbO}(\lambda)C_{HbO} + \varepsilon_{HbR}(\lambda)C_{HbR} + \varepsilon_{H_2O}(\lambda)C_{H_2O} \quad (2)$$

Water content was fixed at 80% while HbR, HbO, a, and b where used as free fitting parameters. The source detector separations corresponded to the distances between the holes of the EEG cap that measured for each size of the EEG cap (S, M and L). The fitting range included all points with a number of counts higher than 90% of the peak value on the rising edge of the curve and 1% on the tail. A Levenberg-Marquardt procedure was employed to minimize the least square error between data and model as estimated by the reduced chi-square (χ^2). For comparison with literature data we calculated $\mu_a(\lambda)$ and $\mu_s'(\lambda)$ from the fitted values of HbO and HbR and from a and b, respectively using Eqs. (1) and (2).

The following quality control parameters were applied to each measurement: number of detected photons >20,000 (for at least 2 out of 3 wavelengths); $\chi^2 \leq 10$; phantom's μ_a or μ_s' values not exceeding the mean ± 2SD of all phantom measurements; $\Delta t_{TDNIRS\text{-}IRF}$ not exceeding mean ± 2SD of the distribution of $\Delta t_{TDNIRS\text{-}IRF}$ in our cohort.

One-way repeated-measure ANOVA was used to evaluate reproducibility considering the three head areas of right and left hemisphere. According to Bonferroni correction, we set the significance level cut-off at $p<0.008$. The square root of residual mean square obtained from one-way repeated-measure ANOVA corresponds to the pooled within-subject standard deviation (SD_w), which represents the intra-subject variation in the measurements [17,35]. The Bland-Altman (95%) repeatability limit, which is the expected maximum difference between two measurements on the same subject in 95% pairs of observations, was calculated according to the following equation [17,35]:

$$RL = \sqrt{2} * 1.96 * SD_w \quad (3)$$

where RL is the repeatability limit, SD_w is the within-subject standard deviation calculated as described before. The RL was proposed by Bland and Altman as a simple way to present measurement errors in reproducibility studies and has been used in previous studies [17,35,36]. Data analyses were performed with SPSS Statistics for Macintosh, version 20.0 (Armonk: IBM Corp.).

3. Results

Measurements were performed on a cohort of 88 subjects (56 male, 32 female). The mean age was 59.8 years old (range 24-89), distributed per decade as reported in Table 2. All subjects were Caucasian.

Mean (±SD) phantoms' values were 0.094 (± 0.002) cm^{-1} for μ_a(690 nm), 0.089 (± 0.006) cm^{-1} for μ_a(785 nm), 0.087 (± 0.004) cm^{-1} for μ_a(830 nm), 8.4 (± 0.5) cm^{-1} for μ_s'(690 nm), 7.2 (± 0.3) cm^{-1} for μ_s'(785 nm) and 6.8 (± 0.3) cm^{-1} for μ_s'(830 nm). Overall quality controls yielded to exclusion of 287 (18.4%) out of 1,561 measurements. In details, 2 measurements (0.1%) were excluded because of low photon counts, 135 (8.6%) for $\chi^2>10$, 90 (5.8%) because of phantom quality control criteria, 60 (3.8%) because the shift interval ($\Delta t_{TDNIRS\text{-}IRF}$) exceeded the accepted range of mean ± 2SD of $\Delta t_{TDNIRS\text{-}IRF}$ distribution (293.5-1072.6 ps). Overall, 34 measurements met more than one quality control criteria. Quality control criteria yielded to the exclusion of 9 subjects (10.2%), leaving 79 subjects in the final analyses.

Biomedical Optics EXPRESS

Table 2. Demographic data of the enrolled subjects

Age (y)	Mean age ± SD	N.	N. Males	N. Females
20-29	26.7 ± 1.7	9	4	5
30-39	32.2 ± 2.6	7	4	3
40-49	44.3 ± 2.9	7	4	3
50-59	54.9 ± 3.1	13	10	3
60-69	63.5 ± 2.8	22	15	7
70-79	74.6 ± 3.3	25	17	8
80-89	84.2 ± 4.4	5	2	3
20-89	59.8 ± 17.3	88	56	32

3.1 Reproducibility analysis

Among the three recording sessions of each subject HbR, HbO, HbT and StO_2 values obtained from each position did not show significant intra-subject difference (Table 3). The SD_w (within-subject variation) was ≤4.1% for StO_2 and ≤7% for HbR, HbO, HbT (Table 3). The intra-class correlation coefficients (ICC) demonstrated an excellent reliability of repeated measurements for μ_a(690 nm), μ_a(785 nm), μ_a(830 nm), HbR, HbO, HbT and StO_2 variables (ICC>0.8) in each position (Tables 3, 4). The ICCs for μ_s'(690 nm), μ_s'(785 nm), μ_s'(830 nm) showed instead a fair to good reliability (ICC 0.5-0.7) (Table 5). The Bland-Altman plots of the TD-NIRS values of the different hemoglobin species indicate a small interval of variation between the three recordings (Fig. 3). After quality control the SD_w (within-subject variation) improved from 8.9% to 4.4% for HbR, from 11.1% to 5.6% for HbO, from 7.5% to 3.8% for HbT, from 7.3% to 2.7% for StO_2.

Table 3. Repeated measures ANOVA: reproducibility of hemoglobin species and StO_2 for each position

				Within-subject effect = Time (3 measurements)			
Var.	**Pos.**	**N**	**Mean ± SD[a]**	**SD_w[a,b,d]**	**RL[a,c,d]**	**p**	**ICC (CI 95%)**
	F3-F5	63	23.9 ± 5.7	1.2 (5.2%)	3.4 (14.3%)	0.095	0.96 (0.95-0.98)
	F4-F6	71	23.6 ± 6.6	1.1 (4.8%)	3.2 (13.4%)	0.078	0.97 (0.96-0.98)
HbR	C3-C1	67	26 ± 7.7	0.9 (3.6%)	2.6 (9.9%)	0.663	0.99 (0.98-0.99)
(µM)	C4-C2	55	25.3 ± 7.2	0.8 (3.3%)	2.3 (9%)	0.233	0.99 (0.98-0.99)
	P3-P5	56	21.2 ± 6.4	1.2 (5.9%)	3.4 (16.3%)	0.008	0.98 (0.96-0.98)
	P4-P6	70	21.7 ± 7.1	1.2 (5.5%)	3.3 (15.2%)	0.167	0.97 (0.96-0.98)
	F3-F5	63	33.8 ± 8	1.4 (4.3%)	4 (11.8%)	0.065	0.97 (0.95-0.98)
	F4-F6	71	32.9 ± 9.8	2.1 (6.3%)	5.7 (17.5%)	0.155	0.96 (0.94-0.97)
HbO	C3-C1	67	35.7 ± 9.9	2.3 (6.3%)	6.2 (17.5%)	0.676	0.96 (0.94-0.97)
(µM)	C4-C2	55	34.6 ± 8.8	2 (5.7%)	5.5 (15.9%)	0.384	0.96 (0.94-0.98)
	P3-P5	56	29.2 ± 9.5	1.5 (5.3%)	4.2 (14.6%)	0.119	0.97 (0.96-0.98)
	P4-P6	70	30.2 ± 9.3	2.1 (6.9%)	5.8 (19.1%)	0.107	0.96 (0.93-0.97)
	F3-F5	63	57.7 ± 12.8	2.4 (4.1%)	6.5 (11.3%)	0.048	0.97 (0.96-0.98)
	F4-F6	71	56.5 ± 15.4	2.1 (3.7%)	5.8 (10.3%)	0.015	0.98 (0.97-0.99)
HbT	C3-C1	67	61.8 ± 16.9	1.9 (3.1%)	5.3 (8.6%)	0.38	0.99 (0.98-0.99)
(µM)	C4-C2	55	59.8 ± 15.4	2.4 (4%)	6.6 (11%)	0.439	0.98 (0.97-0.99)
	P3-P5	56	50.4 ± 15.5	2.5 (4.9%)	6.9 (13.7%)	0.041	0.98 (0.97-0.99)
	P4-P6	70	51.9 ± 15.6	2.2 (4.3%)	6.1 (11.8%)	0.074	0.98 (0.97-0.99)
	F3-F5	63	58.5 ± 4.3	1.1 (1.8%)	3 (5.1%)	0.295	0.94 (0.91-0.96)
	F4-F6	71	57.9 ± 4.9	1.6 (2.8%)	4.5 (7.7%)	0.962	0.89 (0.84-0.93)
StO_2	C3-C1	67	57.8 ± 3.9	1.5 (2.7%)	4.3 (7.4%)	0.866	0.84 (0.77-0.89)
(%)	C4-C2	55	57.8 ± 3.7	1.2 (2.1%)	3.4 (5.9%)	0.188	0.89 (0.84-0.93)
	P3-P5	56	57.6 ± 4.3	1.2 (2.2%)	3.4 (6%)	0.084	0.92 (0.87-0.95)
	P4-P6	70	58 ± 4.8	2.4 (4.1%)	6.6 (11.4%)	0.453	0.8 (0.71-0.86)

[a] Units are shown in the first column; [b] SD_w = within-subject standard deviation (square root of mean square of residuals from one-way repeated measures ANOVA); [c] RL = Repeatability Limit [(expected maximum difference between two measurements in 95% pairs of observations, see Eq. (3)]; [d] in brackets: percentage respect to the mean of the dependent variable; Var. = Variable; Pos. = Position; N = number of valid subjects for analysis, for which none of the 3 measurements were excluded for quality controls; p = p-value of statistical significance to test the null hypothesis H_0: measurement 1 = measurement 2 = measurement 3 (threshold p<0.008). ICC (CI 95%): intra-class correlation coefficient (lower and upper limit of confidence interval at 95%).

Biomedical Optics EXPRESS

Table 4. Repeated measures ANOVA: reproducibility of absorption coefficient (μ_a) for each position

				Within-subject effect = Time (3 measurements)			
λ	**Pos.**	**N**	**Mean ± SD[a]**	**SD_w[a,b,d]**	**RL[a,c,d]**	**p**	**ICC (CI 95%)**
690 nm	F3-F5	63	0.14 ± 0.032	0.005 (3.9%)	0.015 (10.7%)	0.042	0.98 (0.96-0.98)
	F4-F6	71	0.139 ± 0.038	0.005 (3.3%)	0.013 (9.2%)	0.001	0.99 (0.98-0.99)
	C3-C1	67	0.157 ± 0.051	0.01 (6.1%)	0.027 (16.9%)	0.137	0.98 (0.97-0.99)
	C4-C2	55	0.15 ± 0.047	0.009 (5.9%)	0.025 (16.4%)	0.514	0.98 (0.96-0.98)
	P3-P5	56	0.126 ± 0.04	0.007 (5.5%)	0.019 (15.1%)	0.006	0.98 (0.97-0.99)
	P4-P6	70	0.131 ± 0.041	0.005 (3.6%)	0.013 (10.1%)	0.058	0.99 (0.98-0.99)
785 nm	F3-F5	63	0.128 ± 0.024	0.004 (3.4%)	0.012 (9.3%)	0.071	0.99 (0.99-0.99)
	F4-F6	71	0.123 ± 0.029	0.004 (3.1%)	0.011 (8.6%)	0.03	0.99 (0.99-1)
	C3-C1	67	0.133 ± 0.032	0.004 (2.8%)	0.01 (7.8%)	0.17	1 (0.99-1)
	C4-C2	55	0.132 ± 0.029	0.004 (2.9%)	0.011 (8%)	0.803	1 (0.99-1)
	P3-P5	56	0.113 ± 0.029	0.005 (4.4%)	0.014 (12.3%)	0.025	0.99 (0.99-1)
	P4-P6	70	0.114 ± 0.03	0.004 (3.5%)	0.011 (9.8%)	0.299	0.99 (0.99-1)
830 nm	F3-F5	63	0.138 ± 0.027	0.004 (3.2%)	0.012 (9%)	0.063	0.98 (0.96-0.98)
	F4-F6	71	0.134 ± 0.031	0.004 (3%)	0.011 (8.2%)	0.011	0.98 (0.98-0.99)
	C3-C1	67	0.145 ± 0.033	0.004 (2.9%)	0.012 (8%)	0.24	0.99 (0.98-0.99)
	C4-C2	55	0.143 ± 0.031	0.005 (3.5%)	0.014 (9.6%)	0.61	0.98 (0.97-0.99)
	P3-P5	56	0.124 ± 0.032	0.005 (4.4%)	0.015 (12.2%)	0.09	0.98 (0.97-0.99)
	P4-P6	70	0.127 ± 0.031	0.005 (3.6%)	0.012 (9.8%)	0.35	0.98 (0.97-0.99)

[a, b, c, d] Same as Table 3

Table 5. Repeated measures ANOVA: reproducibility of reduced scattering coefficient (μ_s') for each position

				Within-subject effect = Time (3 measurements)			
λ	**Pos.**	**N**	**Mean ± SD[a]**	**SD_w[a,b,d]**	**RL[a,c,d]**	**p**	**ICC (CI 95%)**
690 nm	F3-F5	63	9.8 ± 2	1.2 (11.8%)	3.2 (32.6%)	0.073	0.67 (0.55-0.77)
	F4-F6	71	8.3 ± 1.8	1.1 (12.7%)	2.9 (35.2%)	0.01	0.65 (0.53-0.75)
	C3-C1	67	8.5 ± 1.5	0.8 (9.6%)	2.3 (26.5%)	0.011	0.7 (0.59-0.79)
	C4-C2	55	8.2 ± 1.5	0.8 (10.2%)	2.3 (28.2%)	0.587	0.7 (0.58-0.8)
	P3-P5	56	8.4 ± 1.8	1.3 (15%)	3.5 (41.5%)	0.018	0.6 (0.45-0.72)
	P4-P6	70	7 ± 1.9	1.1 (15.8%)	3.1 (43.7%)	0.444	0.65 (0.54-0.75)
785 nm	F3-F5	63	9.3 ± 2.1	1.1 (12.3%)	3.2 (34.1%)	0.39	0.7 (0.58-0.79)
	F4-F6	71	6.7 ± 1.6	0.9 (13.9%)	2.6 (38.5%)	0.105	0.66 (0.55-0.76)
	C3-C1	67	7.4 ± 1.4	0.8 (10.8%)	2.2 (29.8%)	0.01	0.67 (0.56-0.77)
	C4-C2	55	8.2 ± 1.5	0.8 (9.7%)	2.2 (26.8%)	0.481	0.74 (0.62-0.83)
	P3-P5	56	8.4 ± 1.8	1.2 (14.6%)	3.4 (40.4%)	0.038	0.59 (0.45-0.72)
	P4-P6	70	5.6 ± 1.8	1 (17%)	2.7 (47%)	0.25	0.71 (0.61-0.8)
830 nm	F3-F5	63	8.5 ± 1.8	1 (12.3%)	2.9 (34%)	0.25	0.65 (0.52-0.76)
	F4-F6	71	6.6 ± 1.4	0.9 (13.1%)	2.4 (36.4%)	0.018	0.64 (0.52-0.74)
	C3-C1	67	7.2 ± 1.3	0.7 (9.9%)	2 (27.4%)	0.026	0.68 (0.57-0.78)
	C4-C2	55	7.5 ± 1.3	0.7 (9.8%)	2 (27.2%)	0.473	0.71 (0.59-0.8)
	P3-P5	56	7.7 ± 1.6	1.2 (15%)	3.2 (41.5%)	0.038	0.56 (0.41-0.69)
	P4-P6	70	6 ± 1.6	0.9 (15.7%)	2.6 (43.5%)	0.268	0.66 (0.55-0.76)

[a, b, c, d] Same as Table 3

Biomedical Optics EXPRESS

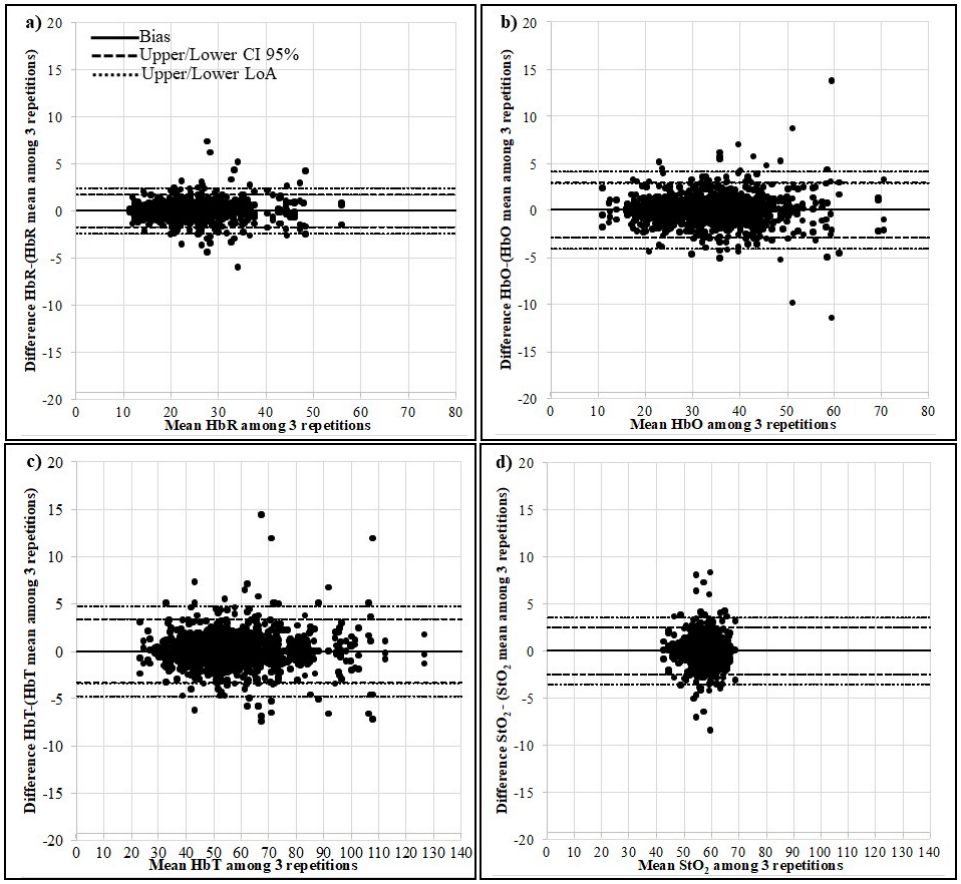

Fig. 3. Bland-Altman plots for HbR (a), HbO (b), HbT (c), StO_2 (d). Each dot represents one recording position for each individual; x-axis: mean value between the 3 measurements for each recording position (units are µM for a, b and c, % for d); y-axis: difference between one measurement and the mean of the 3 recordings (units are µM for a, b and c; % for d). Legend: Bias: average value of y-axis; Upper LoA: Upper Limit of Agreement (bias + 2.77*standard deviation); Lower LoA: Lower Limit of Agreement (bias-2.77*standard deviation) [36].

3.2 Optical properties, hemoglobin species and their variability in the study cohort

The mean (CI 95%) concentrations (µM) of HbR, HbO, HbT and StO_2 (%) and optical properties are reported in Tables 6 and 7. Mean values, standard deviation and CI 95% of cerebral hemispheres and head regions are also reported in Tables 6 and 7. The two cerebral hemispheres displayed similar variability of HbR, HbO, HbT, StO_2 (respectively, $p = 0.371$; $p = 0.257$; $p = 0.281$; $p = 0.726$). Head regions displayed comparable values of StO_2 (%) ($p = 0.619$) but significantly different concentrations of HbR, HbO and HbT (respectively, $p<0.001$; $p<0.001$; $p<0.001$).

We observed inverse correlation between age and HbR, HbO, HbT, StO_2 (respectively, Pearson coefficient $r = –0.31$, $p = 0.006$; $r = –0.47$, $p<0.001$; $r = –041$, $p<0.001$; $r = –0.29$, $p = 0.009$). The observed reduction of HbR, HbO, HbT beginning from the fifth decade (Fig. 4) suggested to split the analysis in two age groups (<55 and ≥55 years old) (Table 8), since subjects older than 55 years had significantly different values of HbR ($p = 0.012$), HbO ($p<0.001$), HbT ($p = 0.001$), StO_2 ($p = 0.036$) compared to younger subjects. Considering subjects older than 55 years, with fairly large sample size ($n = 56$), the coefficient of variation (CV = standard deviation/mean) for StO_2 was 7.7% and ranged between 25.6 and 27.2% for HbR, HbO, HbT.

Biomedical Optics EXPRESS

Table 6. Mean values of hemoglobin species in different head regions

	HbR (µM)	HbO (µM)	HbT (µM)	StO_2 (%)
Global	24.0±7.0 (23.4-24.6)	33.3±9.5 (32.5-34.2)	57.4±15.8 (55.9-58.8)	58.0±4.2 (57.6-58.4)
Left h.	24.3±6.9 (23.4-25.2)	33.9±9.6 (32.6-35.1)	58.2±15.9 (56.2-60.3)	58.1±4.1 (57.5-58.6)
Right h.	23.7±7.1 (22.8-24.7)	32.9±9.5 (31.6-34.1)	56.6±15.8 (54.6-58.7)	57.9±4.4 (57.4-58.5)
Frontal	24.3±6.2 (23.3-25.3)	34.2±9.1 (32.7 35.6)	58.5±14.4 (56.2-60.7)	58.2±4.5 (57.5-59)
Central	25.9±7.4 (24.7-27.1)	35.4±9.5 (33.9-37)	61.3±16.4 (58.7-63.9)	57.8±3.7 (57.2-58.4)
Parietal	21.9±6.8 (20.9-23)	30.6±9.5 (29-32.1)	52.5±15.6 (50-55)	58±4.4 (57.3-58.7)

Mean concentrations of HbR, HbO, HbT are expressed in µM ± Standard Deviation (lower and upper limits of confidence interval at 95% in brackets); mean absolute StO_2 is expressed as % ± standard deviation (lower and upper limits of confidence interval at 95% in brackets).

Table 7. Mean values of optical properties in different head regions

	μ_a (cm^{-1})			μ_s' (cm^{-1})		
	690 nm	**785 nm**	**830 nm**	**690 nm**	**785 nm**	**830 nm**
Global	0.144 ± 0.043 (0.140-0.148)	0.126 ± 0.030 (0.123-0.129)	0.137 ± 0.032 (0.134-0.140)	8.3 ± 1.8 (8.1-8.5)	7.5 ± 1.9 (7.3-7.7)	7.2 ± 1.6 (7.0-7.3)
Left h.	0.145 ± 0.044 (0.139-0.151)	0.128 ± 0.030 (0.124-0.132)	0.139 ± 0.032 (0.135-0.143)	8.8 ± 1.7 (8.6-9.1)	8.3 ± 1.8 (8.1-8.5)	7.7 ± 1.5 (7.5-7.9)
Right h.	0.142 ± 0.043 (0.137-0.148)	0.124 ± 0.030 (0.120-0.128)	0.136 ± 0.032 (0.132-0.140)	7.8 ± 1.7 (7.6-8)	6.8 ± 1.8 (6.5-7)	6.6 ± 1.5 (6.4-6.8)
Frontal	0.144 ± 0.037 (0.138-0.150)	0.128 ± 0.027 (0.123-0.132)	0.139 ± 0.029 (0.134-0.143)	9.0 ± 1.8 (8.7-9.2)	7.9 ± 2.1 (7.6-8.2)	7.5 ± 1.7 (7.2-7.7)
Central	0.155 ± 0.049 (0.147-0.163)	0.134 ± 0.031 (0.129-0.139)	0.145 ± 0.033 (0.140-0.150)	8.4 ± 1.4 (8.2-8.6)	7.8 ± 1.4 (7.6-8)	7.3 ± 1.2 (7.2-7.5)
Parietal	0.132 ± 0.041 (0.126-0.139)	0.116 ± 0.030 (0.112-0.121)	0.128 ± 0.031 (0.123-0.133)	7.6 ± 1.8 (7.3-7.8)	6.9 ± 2.1 (6.5-7.2)	6.7 ± 1.7 (6.4-7)

Mean μ_a and μ_s' are expressed in cm^{-1} ± standard deviation (lower and upper limits of confidence interval at 95% in brackets).

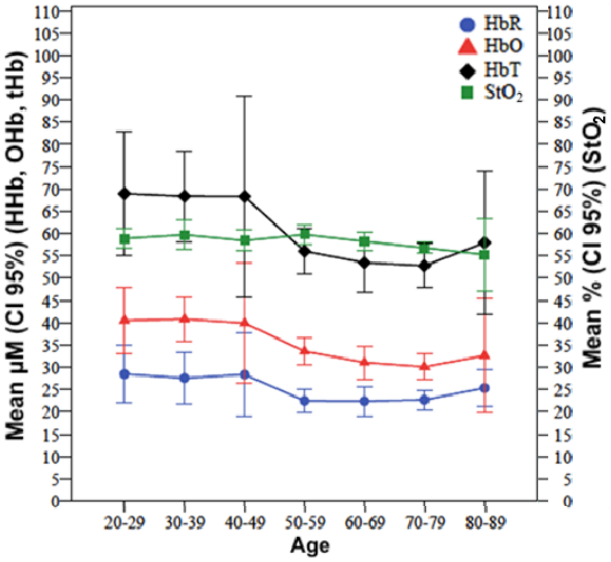

Fig. 4. Line plot of mean values in different age decades. Symbols represent mean values at that decade for each hemoglobin species and oxygen saturation. Mean concentrations of HbR, HbO, HbT are expressed in µM (y axis on the left); mean values of StO_2 are expressed as % (y axis on the right). Error bars represents CI 95%.

Biomedical Optics EXPRESS

Table 8. Global mean values of hemoglobin species and optical properties in two age groups

	<55 years old (n = 23)	≥55 years old (n = 56)	p
HbR (µM)	27.0±8.1 (25.6-28.4)	22.9±6.2 (22.3-23.6)	0.012
HbO (µM)	39.3±9.8 (37.5-41)	31.2±8.5 (30.3-32.1)	<0.001
HbT (µM)	66.3±17.3 (63.2-69.4)	54.1±13.9 (52.6-55.6)	<0.001
StO_2 (%)	59.4±3.4 (58.8-60.1)	57.4±4.4 (57.0-57.9)	0.036
$\mu_a(690)$ (cm^{-1})	0.164±0.052 (0.155-0.174)	0.136±0.037 (0.132-0.140)	<0.001
$\mu_a(785)$ (cm^{-1})	0.142±0.033 (0.136-0.148)	0.12±0.027 (0.117-0.123)	<0.001
$\mu_a(830)$ (cm^{-1})	0.156±0.035 (0.150-0.162)	0.13±0.027 (0.127-0.133)	<0.001
$\mu_s'(690)$ (cm^{-1})	8.3±1.9 (8-8.7)	8.3±1.7 (8.1-8.5)	>0.05
$\mu_s'(785)$ (cm^{-1})	7.5±2.0 (7.2-7.9)	7.5±1.9 (7.3-7.7)	>0.05
$\mu_s'(830)$ (cm^{-1})	7.2±1.6 (6.9-7.4)	7.2±1.6 (7.0-7.3)	>0.05

Values are expressed as mean ± standard deviation (lower and upper limits of confidence interval at 95% in brackets).

4. Discussion

To the best of our knowledge, this is the first study on a large cohort of healthy adult subjects that assessed TD-NIRS short-term reproducibility of absolute values of HbR, HbO, HbT, StO_2, μ_a and μ_s'. Optical properties and hemoglobin parameters displayed non-significant differences among repetitions, with StO_2 showing the lowest within-subject variation ranging from 1.8% to 4.1%. While large studies have reported reference values of NIRS measurements in the newborns [37], few data are available in adults (Table 1). We report optical properties (μ_a, μ_s') and hemoglobin species (HbR, HbO, HbT, StO_2) obtained with TD-NIRS from different head regions of adult subjects.

We acknowledge the use of a homogenous model instead of a two-layer algorithm as a possible limitation of our study. The reason for using a homogeneous model stems from the observation that in a previous multi-laboratory study [16], a substantial agreement was found, both in simulations and *in vivo* measurements, between TD-NIRS absorption coefficients retrieved from the homogenous model and the estimate of the absorption coefficient in the lower layer derived by exploiting a two-layer model.

Our results compare to TD-NIRS data by Auger et al. [8], recorded from the forehead of 18 subjects, aged 18 to 30 years, with a two-layer model that separates the contribution of cerebral and extra-cranial tissue. Although the two study populations are not exactly the same, subjects younger than 55 years in our study, analyzed with homogeneous semi-infinite model, have values close to those from the cerebral layers of Auger et al. (respectively HbR 27 vs. 27 µM, HbO 39.3 vs. 38 µM, HbT 66.3 vs. 65 µM, StO_2 59.4 vs. 58%) [8]. This agreement might further support the assumption that TD-NIRS measurements analyzed by exploiting a homogeneous model for the head reflect mainly cerebral tissue properties. This observation might suggest considering carefully the trade-off between the improved separation of the extra-cerebral tissues by means of a two-layer model and the higher computational resources needed compared to a simpler homogenous model. Indeed, future studies might address this topic in more details.

The mean StO_2 (58%) of our study also compares to the studies of Hallacoglu et al. (58% and 52% in young and elderly subjects respectively) [11], Gatto et al. (57%) [12], Gagnon (60%) [9] and Moreau et al. (63%) [14]. These results might appear unexpected considering previous studies reporting a StO_2 of 44-69% from jugular bulb venous oximetry in adults [38,39] and an estimated arterial fraction of cerebral blood volume of 30% from PET studies [40]. Substantial differences in the object of the investigation between the two techniques might explain this apparent discrepancy. Indeed, while the jugular venous system drains venous blood from the whole brain tissue (white and gray matter as well as superficial and

Biomedical Optics EXPRESS

deep brain structures), TD-NIRS investigates almost only the microcirculation of the grey matter. Since the metabolism of cerebral cortex is roughly two to three times that of the white matter [41,42], cortical venous blood may display lower StO_2 due to higher oxygen extraction compared to other brain regions. On the other hand, the potential impact of the superior sagittal sinus in lowering StO_2 should be negligible according to the following considerations: the main signal of TD-NIRS should come from the microcirculation since large venous structures would hugely absorb injected photons; the distance of ≈3 cm from midline position (Cz) to C1 or C2; the central regions exhibited values of StO_2 comparable to the other head regions. Nevertheless, we observed significant differences in hemoglobin species concentrations among different head regions. In a speculative way, we can hypothesize that these differences might be due to variability in cerebral blood volume, cerebral blood flow and metabolism among different head areas. According to previous PET and MRI studies, a default mode network regulates the activation and deactivation of cerebral regions in resting conditions [43]. The P3-P5 and P4-P6 areas should in part involve the Broadman area 19 [29], which deactivates in resting conditions in the context of default mode network [43]. Parietal regions also exhibited significantly reduced concentrations of HbR and HbO respect to frontal and central regions that were more similar for concentrations of HbR and HbO. The inter-subject variability for the hemoglobin species found in our study cohort needs confirmation in future studies with a larger number of subjects.

Previous studies assessed the reproducibility of NIRS on newborns, mostly using CW-NIRS, with contrasting results (2.4-14.8% for StO_2) [19–24]. However, comparison with our study is limited considering the different type of subjects and instrumentations. The only study that assessed the reproducibility of FD-NIRS on adult subjects was performed by Hallacoglu et al. [11]. They found reproducible results according to the reported cross correlation coefficients between measurements taken 5 months apart of ~0.9 for μ_a(690 nm), μ_a(830 nm), HbR, HbO, HbT, ~0.8 for StO_2, ~0.7 and ~0.6 for μ_s'(690 nm) and μ_s'(830 nm) respectively. We tested reproducibility of TD-NIRS measurements in different head regions at short-term, 5 minutes intervals, after removing and repositioning optical fibers. Indeed, NIRS measurements, performed after a short time period, could be influenced by physiological variations in cortical activation. In this regard, previous fMRI, fMRI-NIRS and fMRI-EEG studies have demonstrated that spontaneous low frequency oscillations (<0.1 Hz) do occur at rest and could be related to changes in blood oxygenation and blood flow [43–47]. Besides, it is recognized that cognitive activity is still present in resting condition and even during sleep [47].

Despite differences in study protocol, we found ICC coefficients ranging from 0.95 to 0.99 for μ_a(690 nm), μ_a(785 nm), μ_a(830 nm), HbR, HbO, HbT and from 0.8 to 0.94 for StO_2 similar to the study of Hallacoglu and colleagues [11]. Compared to previous studies, we tested more head regions, which might increase the consistency of our results.

Our results suggest that HbR, HbO, HbT and, to a lesser extent, StO_2 values reduce with increasing age. Since we are investigating only a limited portion of the brain, in particular the cerebral cortex of six brain regions, we cannot infer on the modifications of global metabolic and hemodynamic cerebral properties that occur with aging. Nevertheless, we know that a number of confounding factors, including atrophy, might become relevant to cerebral metabolism with aging. Indeed, other imaging modalities, such as PET or MRI, reported a progressive reduction of cerebral metabolic rate of oxygen with increasing age without concomitant modifications of oxygen extraction fraction [41, 48–53]. Moreover, the effect of age on cerebral blood flow and cerebral blood volume is controversial as it has been shown that increasing atrophy might be a significant confounding factor [49,51,54–57]. The reduction in HbT may suggest either a decrease in cerebral blood volume and flow, as well as an effect of increasing atrophy [58–60], hemodilution [61] or flow redistribution. In our study the decline of HbR, HbO, HbT and, to a lesser extent, StO_2 appeared more evident after the 5th decade. Although this is an exploratory cut-off, which needs further confirmation,

Biomedical Optics EXPRESS

from a biological point of view it appears appropriate to account for aging. TD-NIRS values of cerebral hemispheres and across brain's regions will be instrumental in planning future studies on neurological diseases, such as acute ischemic stroke, because different brain areas are involved in any given patient.

One strength of our study is the selection criteria of subjects. We gathered medical history and performed neurological examination to exclude relevant neurological comorbidities. In addition, each subject underwent Doppler ultrasonography screening to exclude individuals with ≥50% stenosis of extra- and intra-cranial arteries. We also reviewed available neuroimaging, CT or MRI head scans, which allowed us to exclude significant intra-cranial pathologies. Twenty-six subjects without neuroimaging displayed comparable HbR, HbO, HbT, and StO_2 mean values compared to the remaining sample [respectively, $p = 0.78$; $p = 0.44$; $p = 0.56$; $p = 0.31$)].

Quality control criteria prevented the inclusion of unreliable measurements. Indeed, we have shown that reproducibility improved after the application of quality control criteria. It is worth mentioning that discard of measurement was related mostly to malfunctioning of the device (quality controls for $\Delta t_{TDNIRS\text{-}IRF}$ and phantom measurements) or to movement artifacts (quality controls for $\Delta t_{TDNIRS\text{-}IRF}$ and $\chi^2>10$) and seldom to low photon counts or hair contamination. The application of these quality control criteria might standardize the measurements of future studies and increase the reproducibility among laboratories.

5. Conclusion

In summary, we have provided evidence that TD-NIRS brain measurements are reproducible and we have reported ranges of normal values for absorption and reduced scattering coefficients, oxy-, deoxy- and total hemoglobin concentrations and oxygen saturation in a large cohort of adult subjects. StO_2 displayed the narrowest range of variability across brain regions. Aging appeared to have an impact on hemoglobin species. The results of this work are pivotal for the application of absolute concentrations assessed by TD-NIRS in research and clinical field of neurological diseases, such as ischemic stroke, neurodegenerative diseases, migraine and epilepsy.

Funding

Ministero dell'Istruzione, dell'Università e della Ricerca, Italy [(bursary for the PhD course in Molecular Medicine-Experimental Neurology (G.G.)].

Acknowledgements

G.G, L.R. and A.T. made substantial contribution to the study conception and design. G.G. and L.R. contributed to the statistical analyses of data, to their interpretation and to the drafting of the manuscript. G.G., M.Z., R.R., D.C., L.S., A.T. contributed to the acquisition of data. M.Z., R.R., D.C., L.S., A.T. contributed to the analysis of TD-NIRS data. All authors contributed to critical comments and revision of the manuscript.

Disclosures

The authors declare that there are no conflicts of interest related to this article.